Bubble plume depths and surface wave development as a control on ambient sound in the ocean

Jim Thomson[1], Jie Yang[1], Robert Taylor[2], E.J. Rainville[1], Kristin Zeiden[1], Luc Rainville[1], Samuel Brenner[1,3], Megan Ballard[2], Meghan F. Cronin[4]

[1]Applied Physics Laboratory, University of Washington, Seattle WA 98117 USA
[2]Applied Research Laboratories, University of Texas at Austin, Austin, TX 78713, USA
[3]Dept. of Earth, Environmental, and Planetary Sciences, Brown University, Providence RI 02912, USA
[4]Pacific Marine Environmental Laboratory, NOAA, Seattle WA, USA

Key Points:

- Underwater sound from 1-10 kHz is usually associated with wind forcing and the generation of bubbles.
- Considering surface waves in addition to surface winds can improve interpretation of underwater sound.
- Wind and wave forcing can be combined to give a proxy estimate for the depth of active and passive bubbles that control underwater sound.

Corresponding author: Jim Thomson, jthomson@apl.washington.edu

Abstract

Wind, wave, and acoustic observations are used to test a scaling for ambient sound levels in the ocean that is based on the relative penetration depth of active bubbles during surface wave breaking. The focus is on acoustic frequencies in the range 1-10 kHz, which are typically scaled by wind speed alone. Wind and wave information are combined in a parametric form to describe the depth of the active bubble layer (which produces sound) relative to the depth of the passive bubble layer (which attenuates sound). The relative depth scaling has a primary dependence on wind speed and a secondary dependence on any departure of significant wave height from fully-developed, open-ocean conditions. The scaling is tested with long time-series observations of winds and waves at Ocean Station Papa (North Pacific Ocean), as well as with a case study with fetch limitation near the island of Jan Mayen (Norwegian Sea). When waves are less developed (e.g., limited by fetch) at a given wind speed, the attenuating layer is relatively thin and the sound levels are higher. The scaling is a plausible explanation for the observed reduction in sound levels during high wind events (winds greater than 15 m/s).

Plain Language Summary

Recordings of sound in the open ocean are usually louder when it is windy. This is because winds cause breaking waves at the surface of the ocean (whitecaps). The bubbles created when waves break cause the increase in sound, but these bubbles can also reduce the sound when they make a foamy layer near the surface. Our study uses measurements of winds, waves, and underwater sound to understand these effects. We show that including wave measurements can improve interpretation of sound in the ocean, relative to using wind measurements alone.

1 Introduction

The level of ambient sound in the ocean at mid-frequencies (1-10 kHz) has long been related to surface wind speed. The classic (Wenz, 1962) curves have provided decades of prognostic estimates for the so-called 'wind noise' that increases with wind speed. Many subsequent updates have followed (Hildebrand et al., 2021), including the recent work of Yang et al. (2023) who show that the level of ambient sound saturates, and even decreases, for wind speeds greater than 15 m/s. This phenomenon is spectral; the saturation occurs first at the higher frequencies (e.g, 10 kHz) for a given wind speed (15 m/s), and progresses to lower frequencies with increasing wind speeds. The frequency dependence suggests a length-scale dependence in either the generation or absorption of the sound. The present study explores surface wave height as an essential length scale for the attenuating layer, based on literature showing this to be the region of persistent turbulence and bubbles (Gemmrich, 2010; Sutherland & Melville, 2015; Thomson et al., 2016). The overall idea is that ambient sound in the ocean is a function of winds *and* waves, rather than winds alone.

Although it is still called 'wind noise', the literature is clear that the generation mechanism for this ambient sound is actually surface wave breaking and subsequent bubble activity. This is perhaps best shown at the coasts, where mid-frequency sound production in the surf zone is closely related to incident wave energy (Deane, 2000). In the open ocean, the relation of mid-frequency ambient sound to the dissipation rate of breaking surface waves was shown by Felizardo and Melville (1995). The relationship is sufficiently clear that Manasseh et al. (2006) used ambient sound to detect and quantify breaking waves. The aim of this paper is to re-connect the 'wind noise' to the breaking wave process by understanding the relative depth of bubble plumes generated under breaking waves, and thus explore a mechanism for the scale-dependent saturation of ambient sound during high wind conditions. There are some parallels in this work for the recent results of Dragan-Górska et al. (2023), who show significant wave control on ambient sound

levels in the Baltic Sea and discuss differences from classic wind dependence that may be caused by fetch-limitation of the wave field.

1.1 Bubble layers

Surface wave breaking generates bubbles, which resonate as they are freshly generated to produce mid-frequency underwater sound (Deane & Stokes, 2002). A large distribution of bubble sizes is generated within the plume beneath each breaking wave. The larger bubbles are active in the turbulent flow and either rise to the surface or collapse (generating more sound). The smaller bubbles do not have sufficient rise velocity and become passive (Na et al., 2016). In high sea states, repeated breaking forms a persistent layer of passive bubbles that can trap sound in a near-surface waveguide (Farmer & Vagle, 1989) and attenuate sound as it propagates (Ainslie, 2005). This persistent bubble layer has been suggested as the cause of reductions in received levels under high winds (Yang et al., 2023).

This paper introduces a simple conceptual model as a competition, or ratio, of the penetration depth of active bubble plumes (which generate sound) to the thickness of the passive bubble layer (which traps and attenuates sound). The framework retains wind speed as a primary variable determining ambient sound, and introduces wave height as a secondary dependence.

Wind speed U is used to prescribe the depth of active bubble plumes, D_{bp} following the recent work of Derakhti et al. (2024). That study used down-looking echosounder measurements to develop a parametric scaling

$$D_{bp} = 0.13U^{1.6} \tag{1}$$

that can be applied to measured wind speeds U at a 10 m reference height ($U = U_{10}$). Direct measurements of bubble plume depths were not collected concurrently with the acoustic measurements of the present study, and thus we rely on the wind speed relation of Eq. 1. Although this may introduce scatter to the analysis, it retains the convention for wind speed to be the primary dependence of ambient sound.

Significant wave height H_s is used as a proxy for the thickness of the passive bubble layer, following the observations of Thomson et al. (2016) showing homogenization of surface turbulence via orbital advection with vertical extent H_s. The significant wave heights H_s is calculated over entire surface gravity wave spectrum ($H_s = 4\sqrt{\int E(f)df}$, where $0.05 < f < 0.5$ Hz), which includes both wind-sea and swell components. This choice is driven by the surface kinematics; passive bubbles are advected by wave orbital motion from the entire surface gravity wave spectrum, even though breaking is primarily a short-wave process (Thomson & Jessup, 2009; Thomson et al., 2013).

Combining these estimates using measured wind speeds and wave heights, the hypothesis to be tested is that sound spectra $S(f)$ have a dependence

$$S(f) \propto \frac{D_{bp}}{H_s} = 0.13\frac{U^{1.6}}{H_s}, \tag{2}$$

where that ratio $\frac{D_{bp}}{H_s}$ is referred to as the relative bubble plume depth. Key to this construct is for H_s to be measured (or forecast with a spectral wave model). Prescription of H_s from a parametric wind dependence would defeat the purpose of this scaling and reduce it to a conventional approach to ambient sound that is purely based on wind speed. Winds and waves in the open ocean are typically highly correlated, such that it can be difficult to separate the distinct effects of one or the other. Indeed, existing wind-speed relations for ambient sound are largely successful because long-term average conditions in the open ocean have 'fully-developed' wave heights (which are wind-speed dependent themselves, following Hasselmann et al. (1973) and Pierson and Moskowitz (1964)).

Observations at synoptic time scales (i.e., hours-to-days) indicate that open-ocean wave heights rarely conform to 'fully-developed' conditions, mostly because of the presence of swell (Portilla-Yandún, n.d.). The long-wave swell components do not participate directly in the wave breaking process (Banner et al., 2002), but swell components are important to setting H_s and the overall surface kinematics (Cifuentes-Lorenzen et al., 2018). Fetch-limitation is another reason for H_s to deviate from pure wind formulations, because waves at a given wind speed grow as a function of the distance (i.e., fetch) from boundaries and the long-waves take the most space and time to develop (Dobson et al., 1989; Schwendeman et al., 2014; Thomson & Rogers, 2014). Refraction in coastal zones may also reduce wave heights relative to fully-developed conditions (Ellenson & Özkan-Haller, 2018). We use wind speed measurements as the proxy for sound *generation*, and we use independent wave height measurements as the proxy for sound *attenuation*.

The present study lacks direct measurements of bubble plume depths by echosounders (Dahl & Jessup, 1985; Dahl, 2000; Strand et al., 2020) or optical methods (Al-Lashi et al., 2016). Instead, the scaling of Derakhti et al. (2024) has prompted a new look at existing data with only wind and wave measurements available. In particular, Derakhti et al. (2024) has already shown that 1) active bubble plumes regularly penetrate to depths 2-3 times H_s, and 2) there is an inflection in the ratio $\frac{D_{bp}}{H_s}$ at high winds (> 15 m/s). The inflection occurs at the same wind speed that ambient sound saturates (Yang et al., 2023), though Derakhti et al. (2024) did not make the connection to ambient sound. The present study explores the high wind regime and the acoustic implications of a distinct change in the relative depth of the sound generation region (D_{bp}) compared with the persistent sound attenuating layer (H_s). This new approach is not intended as a definitive prescriptive model for ambient sound, but rather as motivation to develop ambient sound models that explicitly include surface wave and bubble plume characteristics.

2 Methods

The relation of mid-frequency ambient sound to relative bubble depth is explored using two datasets, both with measured winds, waves, and ambient underwater sound. The first is a long-term record, using two years of mooring data from Ocean Weather Station Papa in the North Pacific Ocean. The second is a short-term record, with two weeks of data from multiple SWIFT drifters in the Norwegian Sea. The drifter dataset includes a unique case study in which SWIFT drifters were placed at various fetch distances downwind of the Jan Mayen volcanic island. The first dataset has the benefit of many realizations; the second dataset has the benefit of distributed sampling and the fetch case study that explicitly changes H_s without changing U_{10} in Eq. 2. The hydrophone depths are quite different between the two datasets (500 vs 10 m, respectively), but the measurements are roughly comparable assuming the ambient sound source behaves as a surface dipole layer, where the acoustic spreading loss resulting from a greater receiver depth is offset by the increased number of observable surface sources (Urick, 1975).

2.1 Ocean Station Papa (North Pacific) moorings

Ocean Weather Station Papa (OWS-P) is located at 50 N, 145 W in the North Pacific Ocean and is one of the longest time series in the world's oceans. Data from this location extend back to the World War II era (Freeland, 2007), including a remarkable dataset of visual wave observations (Belka et al., 2014). The modern data at OWS-P are centered around a series of moorings, including a Datawell waverider maintained by the Applied Physics Laboratory at the University of Washington (Thomson et al., 2013, 2015) and a surface meteorological / upper ocean mooring maintained by the Pacific Marine Environmental Laboratory at the National Oceanographic and Atmospheric Administration (NOAA) (Cronin et al., 2015, 2023). The waverider mooring has been replaced

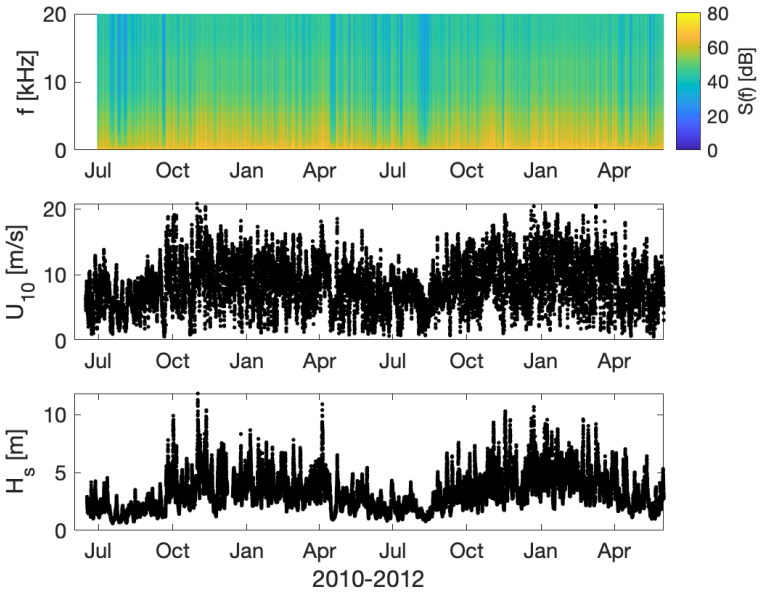

Figure 1. Time series of observations at Ocean Weather Station Papa (OWS-P) from 2010 to 2012. Acoustic spectra (top panel) are measured with a sub-surface PAL. Wind speeds (middle panel) are measured with anemometers on the NOAA surface buoy. Significant wave heights (bottom panel) are measured with a Datawell waverider buoy.

every 1-2 years and usually has included a Passive Aquatic Listener (PAL) at 500 m depth. For this study, we select the period of 2010-2012 and utilize the ambient sound recordings and wave data from the waverider mooring, along with the winds from the NOAA mooring.

Figure 1 are the 2010-2012 time series from OWS-P, which has a strong seasonal signal of storms in winter and mild conditions in summer. All parameters are statistical measures produced hourly: the ensemble ambient sound spectra, the significant wave height from the first moment of the wave energy spectra, and the average wind adjusted to 10 meter reference height. The ensemble sound spectra come from recordings that are 4.5 seconds in duration, at an interval of 8 minutes. The acoustic sampling rate is 100 kHz. The recordings are split into 450 windows with 50% overlap, then spectra from these windows are averaged to produce ensemble spectra every 8 minutes.

2.2 Jan Mayen drifters

Jan Mayen is a volcanic island at the west edge of the Norwegian Sea. Data from this location were collected as part of a 2021 pilot cruise for the Northern Ocean Rapid Surface Evolution (NORSE) project (M. Ballard et al., 2022). Data collection used drifting SWIFT buoys (Thomson, 2012) which measure winds, waves, and turbulence in a wave-following reference frame. For these deployments, two of the SWIFTs included a Loggerhead SNAP hydrophone suspended at a depth of 10 m. The SNAP hydrophone spectra used herein come from recordings that are 60 seconds in duration, at an interval of 300 seconds. The acoustic sampling rate is 48 kHz.The SNAP hydrophone is mounted in a downward orientation, causing the coupled interaction between the electronics housing and the hydrophone, resulting in anomalous features in the acoustic spectra that were

especially evident in the 900 Hz-2 kHz band. This is discussed at length in the appendix, and these bands are interpolated across in the results that follow.

Figure 2 shows the wind and wave conditions measured by the SWIFT buoys during NORSE 2021. The SWIFTs without hydrophones are included to evaluate the widest possible range of $\frac{D_{bp}}{H_s}$, including the effects of reduced fetch in the shadow of Jan Mayen.

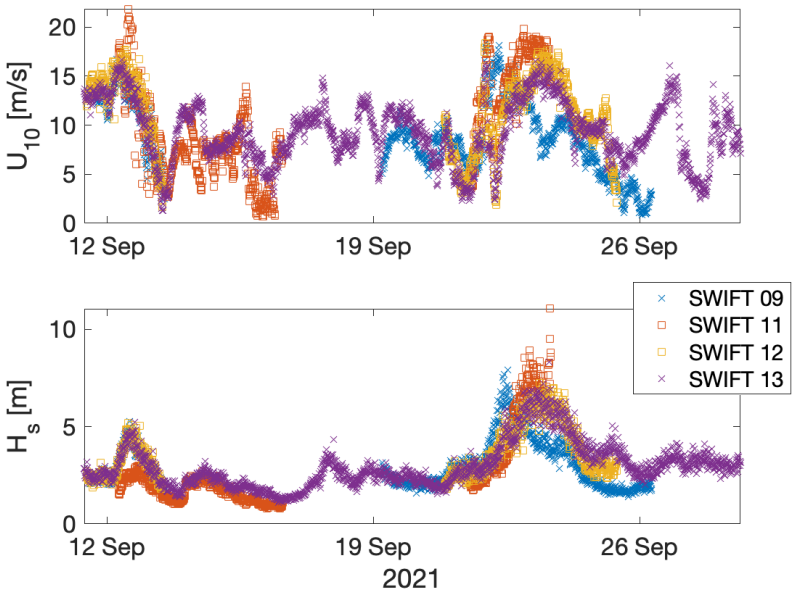

Figure 2. Time series of wind speeds (top panel) and significant wave heights (bottom panel) from drifting SWIFT buoys near the island of Jan Mayen in the Norwegian Sea. Square symbols are used for buoys with hydrophones and crosses are used for buoys without hydrophones. The extreme wave heights from SWIFT 11 on 24 Sep 2021 were measured as it transited the surf zone and beached on Jan Mayen.

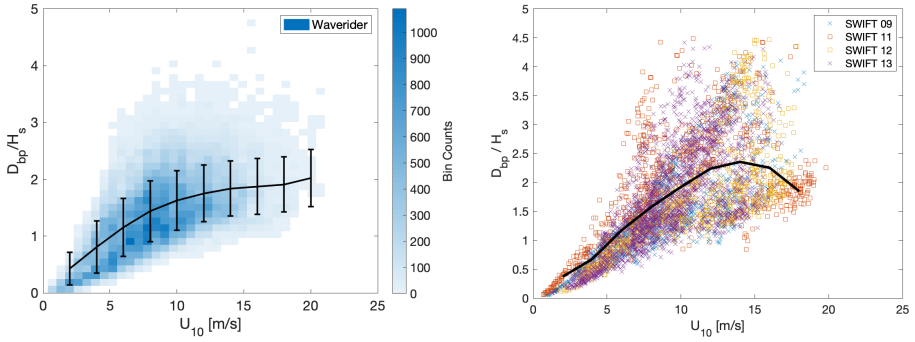

Figure 3. Relative bubble plume depths versus wind speed from two years of waverider observations at OWS-P (left) and two weeks of drifting SWIFTs near Jan Mayen (right). The waverider values are hourly and binned for better visualization; the black line shows means and standard deviations. The SWIFT values are individual symbols every 12 minutes, with a black curve showing binned averages.

3 Results

3.1 Relative bubble plume depths

The wind- and wave-based scaling of $\frac{D_{bp}}{H_s}$ from Eq. 2 is shown for both datasets in Figure 3 as a function of wind speed. There is a general trend for increasing values with wind speed, but there is not a 1:1 correspondence with wind speed. The highest values of relative bubble plume depths are several multiples of the significant wave height and occur around $U_{10} \sim 15$ m/s. There is almost no dependence on wind speed for $U_{10} > 15$ m/s.

The lack of a 1:1 correspondence with wind speed in Figure 3 is essential to this study and to the wave-informed framework. These datasets demonstrate that surface layer thickness (as given by wave height H_s) is not uniquely determined by wind speed, and thus ambient sound level also should not be monotonic nor unique with wind speed. The values from Ocean Weather Station Papa have a wide range of conditions and robust statistics. The values near Jan Mayen have some specific patterns that are related to wave sheltering and fetch limitation on the leeward side of the island; these will be addressed in the case study.

3.2 Binned acoustic spectra

Ensemble acoustic spectra are shown in Figure 4 for OWS-P data and Figure 5 for Jan Mayen data. Each includes a panel (left) using a conventional wind-only approach to bin the ensembles and another panel (right) using the relative bubble plume depth $\frac{D_{bp}}{H_s}$ to bin the ensembles. The wind-only ensembles (left panels) are well-sorted at low winds, but at higher winds the spectra collapse and decrease with increasing frequency. The relative bubble plume depth ensembles (right panels) are well-sorted for all conditions and retain their spectral shape at high frequencies. The sound levels across 1-10 KHz show a robust increase with relative bubble plume depths. The right panels still have a strong wind dependence implicit in the parametric specification of $D_{bp} \approx U^{1.6}$, but the spectra are better sorted because the the attenuating surface layer effects are represented by normalizing the wind speed effects with the wave effects H_s.

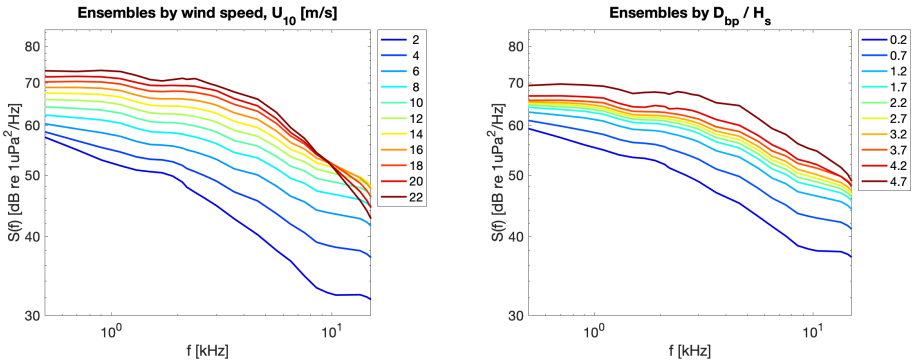

Figure 4. Ensemble acoustic spectra from two years of data at OWS-P that are binned by wind speed (left panel) and by relative bubble plume depth (right panel).

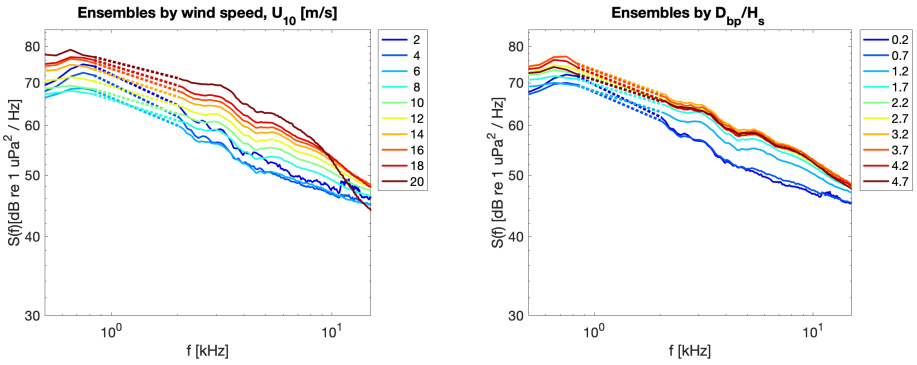

Figure 5. Ensemble acoustic spectra from two weeks of drifter data near Jan Mayen that are binned by wind speed (left panel) and by relative bubble plume depth (right panel). The dashed portion of each curve shows the interpolation across the frequency bands with directional effects (see appendix).

3.3 Fetch-limited case study

The NORSE 2021 pilot experiment sampled a particularly strong wind event for a few days in September 2021, during which four SWIFT buoys were deployed at increasing fetch distances downwind of Jan Mayen. The island acted as a barrier to the local wave field (i.e., the wind sea), such that the fetch is effectively zero at Jan Mayen and increases with distance from the island. As a practical application of this fetch dependence, the R/V Neil Armstrong took shelter at the short fetch behind Jan Mayen during the most intense portion of the event. Figure 6 shows the wave and wind conditions from the four buoys. For the one-hour timeseries used in this case study, the wind is nearly constant at 15 m/s for all of the buoys, but the wave field is a strong function of fetch distance x. This creates a natural laboratory for studying the dependence on wave height distinct from the dependence on wind speed in Eq. 2.

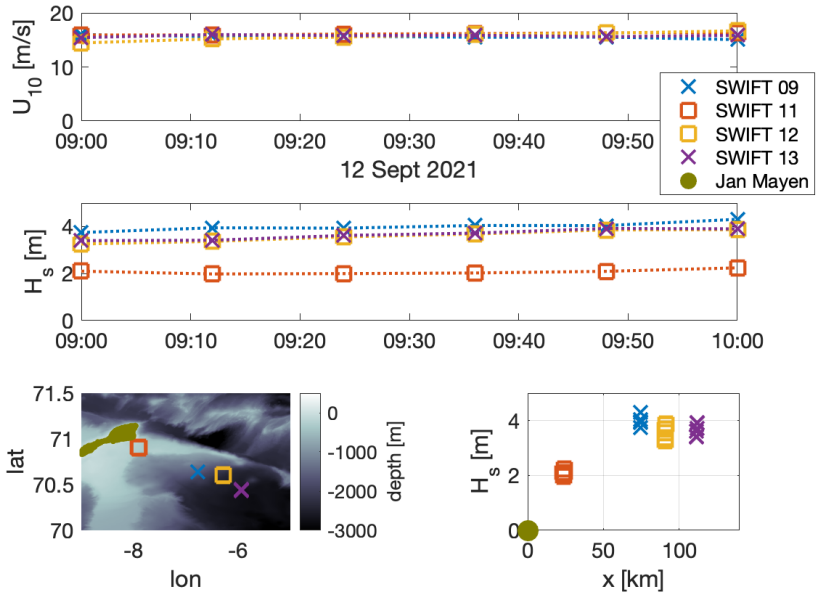

Figure 6. Time series of wind speeds (top panel), significant wave heights (middle panel), and positions (lower left panel) of drifting SWIFT buoys near the island of Jan Mayen. Shading in the lower left panel indicates water depth (green is land). The wind speeds are similar for all buoys, while the wave heights are a strong function of the fetch distance x downwind of the island (lower right panel).

Figure 7 shows the wave conditions scaled by the non-dimensional fetch distance downwind of Jan Mayen. This is a classic analysis in which wind speed U_{10} and gravity g are used to scale the fetch as gx/U_{10}^2 and the wave height as gH_s/U_{10}^2 (Dobson et al., 1989). The expectation is a quasi-linear, or a weak power-law, relation between the non-dimensional variables (Fontaine, 2012; Stiassnie, 2012), which is shown by the dashed line in Figure 7. The observations from this case study are more complex than the classic fetch law, and this is probably because the island does not completely block all of the waves generated upwind of the island. The point is not to achieve a perfect fetch scaling, but rather to show that the differences in wave heights between SWIFT 11 and SWIFT 12 (which have the two hydrophones) are reasonable given the differences in fetch. In particular, there is a clear reason for these two buoys to measure the same wind speed while measuring very different wave heights.

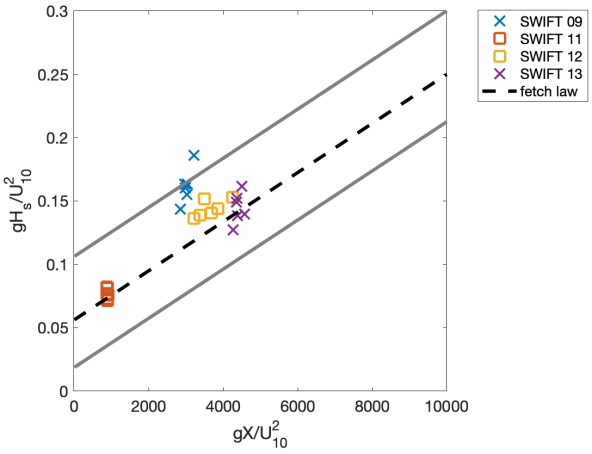

Figure 7. Non-dimensional wave height versus non-dimensional fetch during the Jan Mayen case-study. The dashed line shows the theoretical grow of waves with fetch, assuming steady-state winds and the absence of swell. Gray lines show uncertainty around the theoretical fetch relation.

Figure 8 shows ambient sound spectra from the two SWIFTs with hydrophones downwind of Jan Mayen. Though they have essentially the same wind speed, they have different wave heights (according to a fetch dependence). The qualitative difference is consistent with the relative bubble plume depth hypothesis. If wind speed was the only dependence, the two spectra in Figure 8 would plot on top of each other. At short fetch, measured sound is louder because the active bubble plumes penetrate deeper, relative to the layer of persistent attenuation by passive bubbles that is set by wave height ($D_{bp}/H_s = 3.5$). At long fetch, measured sound is quieter because the attenuation layer is deeper, such that a greater portion of active bubble plumes are confined within the attenuation layer ($D_{bp}/H_s = 1.8$). The fetch dependence is qualitatively similar to the recent results of Dragan-Górska et al. (2023) in the Baltic Sea.

Implicit to this case study is an assumption that the wind scaling for bubble plume depth (Eq. 1) is not itself a function of fetch. This asserts that only H_s changes and D_{bp} does not, because the winds are $U_{10} = 15$ m/s throughout. This assumption is supported by prior work showing that wave breaking is predominantly a short-wave process in balance with the local winds (Thomson & Jessup, 2009; Sutherland & Melville, 2013). This is different from H_s, which integrated over the whole surface wave spectrum. Thus, there is a scale separation between the short waves that break to generate bubble plumes and the longer waves that grow with fetch to control the total H_s (Schwendeman et al., 2014).

4 Discussion

The combined results suggest that ambient sound in the ocean is as a function of winds and waves, rather than winds alone. As with any observational study, there remain numerous other factors to consider.

4.1 Shallow-water effects near Jan Mayen

In contrast to the deep-water conditions of OWS-P, the bathymetry around Jan Mayen is complex and includes shallow regions close to the island (Figure 6). The location of SWIFT 11 relative to Jan Mayen and the direction of the wind results in both

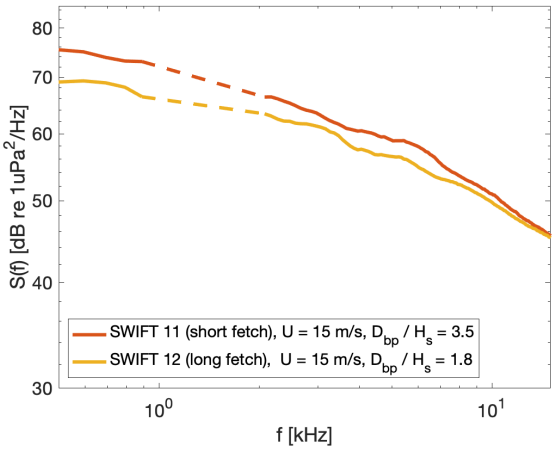

Figure 8. Acoustic spectra from the two SWIFT buoys during the Jan Mayen case study. The buoys observe the same winds, but SWIFT 11 has a larger relative bubble plume depth because of the fetch dependence of wave height. The larger relative depth is associated with higher acoustic levels.

a shorter fetch and a shallower water depth than that of SWIFT 12. Shallow water depths are frequently associated with elevated ambient acoustic spectra (Wenz, 1962). Wenz considered depths less than 100 fathoms ($\sim$ 200 m) to be shallow water[1], and suggested adding 2 to 3 dB to the average empirical wind noise curves in such environments. At a water depth of $\sim$250 m over the duration of the measurements presented, SWIFT 11 is near the transition depth defined by Wenz. Significant differences in both water depth and measured acoustic level between SWIFT 11 and SWIFT 12 warrant an exploration into the impact of water depth on the ambient sound environment.

A range-independent ambient acoustic model was implemented to investigate the influence of the water depth on the ambient sound level. The ray-based model traces the propagation paths that arrive at the receiver for a range of elevation angles $-90° < \theta < 90°$. The model provides the incoherent contribution of all surface dipole sources that reach the receiver, accounting for acoustic absorption and reflection losses along each path. Other than water depth, the model environmental inputs for SWIFT 11 and SWIFT 12 were kept the same.

The empirical Wenz level N_w, a function of both wind speed U and frequency f, was used for the surface dipole strength $N_w \sin\theta/\pi$. The normalization of the surface dipole strength by π enables a return to the input ambient level N_w when integrating over solid angle in a lossless and bottomless isotropic-sound-speed environment(Ainslie, 2010; APL-UW, 1994), representing the acoustic level as measured by an omnidirectional hydrophone. Following the work of M. S. Ballard et al. (2023), the bottom was modeled as a gravel sediment halfspace, providing a fairly reflective fluid bottom with a critical grazing angle of $\sim 30°$. Reflection losses from sea surface interactions were calculated using Ainslie's mid-frequency model (Ainslie, 2005). The sound speed profile used contained a surface duct in the upper 50 m of the water column consistent with measured

[1] This is shallow water in terms of the acoustics, but not in terms of the surface gravity waves. At 200 m, much of the surface gravity wave spectrum is in deep water, though the longer swells are intermediate water depth.

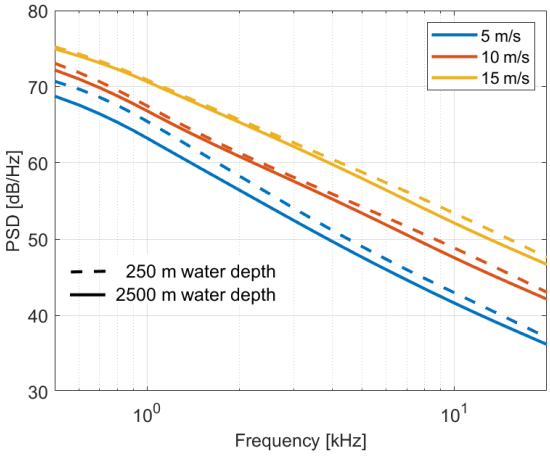

Figure 9. Modeled ambient acoustic spectra for shallow-water and deep-water environments for multiple wind speeds. Increases to the ambient level resulting from the shallower environment are on the order of ~ 1 dB and decrease with increasing wind speeds.

sound speed profiles from the experiment. Model results for the two different environments for several wind speeds are displayed in Figure 9.

In the shallow water environment, the low-loss gravel bottom intensifies the contribution of small grazing angle energy near horizontal that propagates over long distances. However, the modeled differences in spectral level shown in Fig. 9 are not significant enough to explain the measured differences between SWIFT 11 and SWIFT 12, particularly at high wind speeds, where the increase in surface loss prohibits long distance propagation, negating the impact of the reflective bottom. The model's inability to represent the increased ambient acoustic spectral levels measured at SWIFT 11 for the associated wind speeds indicates that water depth is not responsible for the raised levels.

This modeling analysis supports the interpretation that differences in the ambient sound levels are the result of differences in the surface wave conditions (and thus relative bubble plume depth) at the two locations. The significant wave heights at SWIFT 11 are much less than those of for fully-developed conditions in the open ocean (Pierson & Moskowitz, 1964; Hasselmann et al., 1973), because there is insufficient fetch to develop the lower frequency surface waves. The higher frequency surface waves associated with breaking (and active bubble plumes) respond to wind forcing on shorter space and time scales, so the similar wind speeds observed at SWIFT 11 and SWIFT 12 should produce similar active bubble plume depths D_{bp}. The significant wave heights H_s used for the passive layer depth are integrated over the full surface wave spectra, and thus the lack of longer waves at SWIFT 11 creates at different acoustic environment. The fetch-limited conditions at SWIFT 11 are likely responsible for the increase in the relative bubble plume depth, resulting in the greater ambient acoustic spectra when compared with that measured at SWIFT 12.

The historical measurements of Lemon et al. (1984) are also relevant to the question of shallow water effects. That study found elevated ambient sound levels at a coastal site, relative to open ocean levels, for a range of wind speeds (APL-UW, 1994). Although that study did not include wave measurements or consider wave effects, we can review the wind record and estimate that the storm duration was too short to produce fully-developed waves. We can also examine the site and assert that refraction along the coast may have further reduced the wave heights. Applying the scaling of our present study,

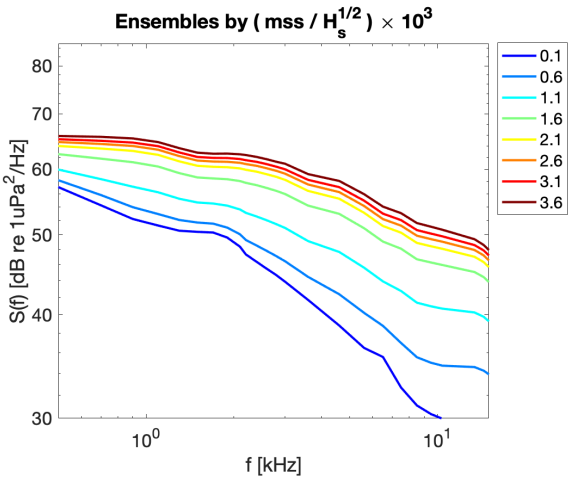

Figure 10. Ensemble acoustic spectra from two years of data at OWS-P that are binned by entirely by wave parameters, using the ratio of mean square slope mss to the square root of the significant wave height $H_s^{1/2}$.

the H_s denominator in Eq. 2 would be smaller for Lemon et al. (1984) than an open ocean H_s. Thus, it would make sense for ambient sound levels to be elevated in that study, because D_{bp}/H_s would be higher for a given wind speed.

4.2 Additional wave effects: limitation of wave slopes at high winds

Other wave characteristics beyond H_s setting the vertical scale of the attenuating layer are also ripe for more examination. The observed saturation of ambient sound (Yang et al., 2023) occurs at the same wind speed ($U_{10} \sim 15$ m/s) for which wave slopes saturate (Davis et al., 2023). A common metric is the mean square slope (mss) of the waves, which is the fourth moment of the scalar wave spectrum and integrates over the wave scales spanning f_1 to f_2,

$$mss = \int_{f1}^{f2} \frac{(2\pi) f^4 E(f)}{g^2} df. \tag{3}$$

We use use $f_1 = 0.2$ Hz and $f_2 = 0.4$ Hz, following prior work relating mss to wave breaking rates (Schwendeman & Thomson, 2014). We thus expected a relation between mss and ambient sound generation. Further, it is now common practice to use mss measured by wave buoys to give a proxy wind speed estimate (Voermans et al., 2020) based on the concept of wind-wave equilibrium (Thomson et al., 2013). Thus, mss is a reasonable parameter to characterize the generation of active bubbles causing ambient sound. Continuing with the total H_s as a parameter characterizing the attenuation of sound by the persistent bubbles, we can define new scaling for ambient sound that is entirely wave-based: the ratio of mss/H_s.

Figure 10 tests a ratio $mss/H_s^{1/2}$ scaling with the 2-year OWS-P dataset. The square root of H_s is used so as to have a dynamic range more similar to the range of mss. The monotonic sorting of ambient sound spectra is similar to the relative bubble plume depth result from before; it is again more monontonic than the conventional wind speed approach. This suggests that wave spectral measurements (and/or models) alone may be useful in prescribing ambient sound levels. This result does not intend to unravel decades of 'wind noise' literature, but rather illuminate the highly coupled wave dynamics that mediate the wind forcing.

5 Conclusions

Mid-frequency ambient sound in the ocean has a primary dependence on wind speed, which is a proxy for surface wave breaking and the generation of active bubble plumes in the upper ocean. This sound likely is attenuated by smaller bubbles, which are persistent in a layer with a proxy depth of one significant wave height (H_s). At high wind speeds (> 15 m/s), this persistent layer becomes significant relative to the active bubble plume depth layer, and the net effect is to attenuate more of the generated sound before it can propagate farther into the ocean. This may explain the observations of Yang et al. (2023), which show a saturation of measured sound for high wind speeds. An empirical scaling for the depth ratio of active and passive bubbles, based on measured winds and waves, is successful in sorting ambient sound spectra and may be useful approach for the future development of prognostic models.

The D_{bp}/H_s scaling may not become a predictive model for ambient sound, and it does not directly address the shape of the ambient sound spectra $S(f)$. Yet it is a clear indicator that including surface waves and bubble plume characteristics can improve predictions relative to wind alone. The bubble plumes that cause sound generation and attenuation need more detailed characterization as a function of wind and wave conditions. In addition to bubble depth penetration and persistence, void fractions and bubble size distributions need to be quantified over the full range of open-ocean and coastal conditions. Such measurements would enable more detailed acoustic propagation modeling, including distinguishing between the passive (small) bubbles and active (large) bubbles. For the common inverse problem of obtaining proxy winds (and rain rates) from ambient acoustic measurements, the results herein provide a framework to explore the scatter in those methods and potential avenues to improve those estimates.

Open Research Section

Station Papa wind data were retrieved from `https://www.pmel.noaa.gov/ocs/Papa`. Station Papa wave data were retrieved from `http://thredds.cdip.ucsd.edu/thredds/catalog/cdip/archive/166p1/catalog.html`. The complete data and processing codes from this work are publicly available at `http://hdl.handle.net/1773/51039`.

Acknowledgments

This research was supported by the Office of Naval Research (Awards N00014-20-1-2417 and N00014-21-1-2743). The waverider mooring at Ocean Station Papa is maintained using NSF support (award OCE-2122317) and the surface wind mooring at Ocean Station Papa is maintained by NOAA PMEL through funding from NOAA's Global Ocean Monitoring and Observing program. This is PMEL paper number 5604.

Appendix A Directionality of Loggerhead SNAP Recorders

The time-averaged ambient sound spectra collected with the Loggerhead Snap recorders showed evidence of anomalous features. The most severe features were in the 900 Hz to 2 kHz band, which were removed from Fig. 5 and replaced with a dashed line representing an interpolation over the affected frequency band. These features were present throughout the data set, independent of wind speed and wave height. These irregularities in the ambient sound spectra were attributed to the acoustic response of the Snap recorders due to the proximity of the hydrophone to the air-filled pressure housing.

The Snap recorder has a PVC housing roughly 0.5 m long and 5 cm in diameter, with the power supply and data acquisition system contained internally. The external HTI 96 hydrophone is connected to the housing by a 3 cm long semi-rigid cable. The

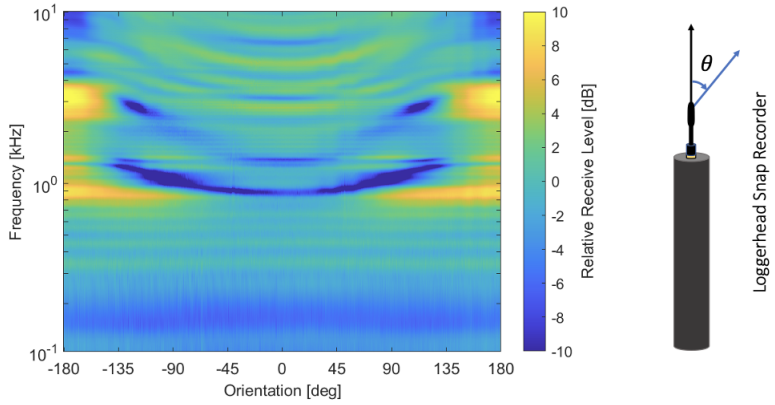

Figure A1. Measured acoustic directivity of the Loggerhead Snap recorder. Positive/negative dB levels indicate the amplification/suppression of received signals at each receiver orientation angle (hydrophone facing source at $\theta = 0°$).

proximity of the hydrophone to the housing, the deployed orientation with the hydrophone pointed away from the sea surface, shadowing and diffraction around the housing, and the acoustic resonances of the cavity are all possible contributing factors to the irregularities observed in the measurements.

To determine the acoustic sensitivity of the Snap recorder as a function of direction and frequency, calibrated measurements were taken at the Lake Travis Test Station in Austin, Texas. The lake bed below the test station has a gradual slope, with an average water depth of 20 m directly below the experimental setup. During testing, the water column consisted of a 30 °C isothermal layer in the upper 12 m, followed by a thermocline reducing the temperature to 20 °C at 20 m. The response of the system is assumed symmetric about the axis of the recorder. To measure the change in response as a function of receive angle θ of the incident sound wave, the Snap recorder was suspended horizontally by 10 m of fishing line, with its axis parallel to the water surface. The fishing line was connected to a rotating column, with the hydrophone centered on the column's axis of rotation.

The Snap recorder collected data continuously at 48 kHz as it was rotated at a speed of approximately 1 deg/s, with the 360° rotation lasting roughly 6 minutes. A Navy standard J9 projector[2] was used for the calibration. It was placed at 10 m depth 1 m from the center of the rotating column. For the J9 projector, far-field propagation is attained roughly 10 cm from the source. The calibration signal was a 10 ms linear frequency modulated chirp from 50 Hz to 20 kHz, repeated every 250 ms. The length of the chirp was chosen to prevent reflections from contaminating the received signal.

Reference measurements of the projector signal were collected with a calibrated Navy standard H56 hydrophone[3] placed at 10 m depth below the rotating column, i.e. in the location previously occupied by the Snap recorder hydrophone. The difference of the received power spectral density level as measured by the reference hydrophone to that measured by the Snap recorder provides the nominal response of the Snap recorder for each receive angle. Figure A1 shows the calibrated acoustic response of the Snap recorder as a function of angle and frequency for the full rotation. Note that a 200 Hz high-pass fil-

[2] `https://www.navsea.navy.mil/Portals/103/Documents/NUWC_Newport/USRD/J9.pdf`
[3] `https://www.navsea.navy.mil/Portals/103/Documents/NUWC_Newport/USRD/H56.pdf`

ter was applied to both the Snap recorder data and the H56 data to remove environmental noise.

The directivity of the Snap recorder is significant, with variations of ± 10 dB at different orientations for many frequencies in the 500 Hz to 4 kHz band. With the deployed orientation facing away from the sea surface, direct path sea surface sound arrives at angles $|\theta| >= 90°$, with sound from directly overhead arriving at $|\theta| = 180°$ and surface generated sound from more distant patches arriving at lower angles. The strong frequency-dependent directionality is an important consideration in the interpretation of ambient sound data collected with the Snap recorders. Compared to the HIFEVA model ambient sound curves (APL-UW, 1994), the spectra shown in Fig. 5 are biased toward higher ambient sound levels. This result is broadly consistent with the measured directivity shown in Fig. A1, which on average shows a higher response in the 500 Hz to 4 kHz range for angles between $\pm 90°$ and $\pm 180°$.

Although only one Snap recorder was calibrated at the Test Station, the overall angle- and frequency-dependence is expected to be consistent between units owing to their similar construction. However, the two Snap recorders used for the NORSE ambient sound measurements showed high-frequency oscillations that were slightly offset from one another between 900 Hz and 2 kHz. These oscillations roughly align with the narrow-band, wide-angle elevated response near 1 kHz in the calibration measurement shown in Fig. A1. Slight variations in the construction and preparation of the Snap recorders could be responsible for small shifts in the characteristics of the acoustic response. These features were removed from Fig. 5 to facilitate a cleaner comparison between the two recorders. While the absolute values of the measurements are influenced by the acoustic response of the recorders, the differences in the observed ambient sound levels between SWIFT 11 and SWIFT 12 can be attributed to differences in the ambient sound generation and propagation environment.

References

Ainslie, M. A. (2005). Effect of wind-generated bubbles on fixed range acoustic attenuation in shallow water at 1–4khz. *The Journal of the Acoustical Society of America*, *118*(6), 3513-3523. Retrieved from `https://doi.org/10.1121/1.2114527` doi: 10.1121/1.2114527

Ainslie, M. A. (2010). *Principles of sonar performance modelling* (Vol. 707). Springer.

Al-Lashi, R. S., Gunn, S. R., & Czerski, H. (2016). Automated processing of oceanic bubble images for measuring bubble size distributions underneath breaking waves. *Journal of Atmospheric and Oceanic Technology*, null. Retrieved from `http://dx.doi.org/10.1175/JTECH-D-15-0222.1` doi: 10.1175/JTECH-D-15-0222.1

APL-UW. (1994). *High-frequency ocean environmental acoustic models handbook* (Tech. Rep. No. TR9407). Applied Physics Laboratory, University of Washington, Seattle, WA.

Ballard, M., MacKinnon, J., Rainville, L., Simmons, H., Abbot, P., Bergentz, K., ... Zeiden, K. (2022). *Northern ocean rapid surface evolution (norse): Science and experiment plan* (Tech. Rep. No. 2102). Applied Physics Laboratory, University of Washington.

Ballard, M. S., Sagers, J. D., Poulain, P.-M., Mackinnon, J., Lucas, A. J., & Sanchez-Rios, A. (2023). Out-of-plane arrivals recorded by drifting hydrophones during the northern ocean rapid surface evolution experiment. *The Journal of the Acoustical Society of America*, *154*(5), 2757–2768.

Banner, M., Gemmrich, J., & Farmer, D. (2002). Multiscale measurements of ocean wave breaking probability. *J. Phys. Oceanogr.*, *32*, 3364-3375.

Belka, D., Schwendeman1, M., Thomson, J., & Cronin, M. (2014). *Historical wave*

and wind observations at ocean station p (Tech. Rep. No. 1407). Applied Physics Laboratory, University of Washington.

Cifuentes-Lorenzen, A., Edson, J. B., & Zappa, C. J. (2018). Air–sea interaction in the southern ocean: Exploring the height of the wave boundary layer at the air–sea interface. *Boundary-Layer Meteorology*, *169*(3), 461–482. Retrieved from https://doi.org/10.1007/s10546-018-0376-0 doi: 10.1007/s10546-018-0376-0

Cronin, M. F., Anderson, N. D., Zhang, D., Berk, P., Wills, S. M., Serra, Y., ... Meinig, C. (2023, October). Pmel ocean climate stations as reference time series and research aggregate devices. *Oceanography*. Retrieved from https://doi.org/10.5670/oceanog.2023.224

Cronin, M. F., Pelland, N. A., Emerson, S. R., & Crawford, W. R. (2015). Estimating diffusivity from the mixed layer heat and salt balances in the north pacific. *Journal of Geophysical Research: Oceans*, *120*(11), 7346-7362. Retrieved from https://agupubs.onlinelibrary.wiley.com/doi/abs/10.1002/2015JC011010 doi: https://doi.org/10.1002/2015JC011010

Dahl, P. (2000). Bubble clouds and their transport within the surf zone as measured with a distributed array of upward-looking sonars. *J. Acoust. Soc. Am.*, *109*(1).

Dahl, P., & Jessup, A. T. (1985). On bubble clouds produced by breaking waves' an event analysis of ocean acoustic measurements. *J. Geophys. Res.*, *100*(C3).

Davis, J., Thomson, J., Houghton, I. A., Doyle3, J. D., Komaromi, W., Fairall, C. W., & Thompson, E. J. (2023). Saturation of ocean surface wave slopes observed during hurricanes. *Geophys. Res. Let.*, *50*. Retrieved from https://doi.org/10.1029/2023GL104139 doi: 10.1029/2023GL104139

Deane, G. B. (2000). Long time-base observations of surf noise. *The Journal of the Acoustical Society of America*, *107*(2), 758-770. Retrieved from https://doi.org/10.1121/1.428259 doi: 10.1121/1.428259

Deane, G. B., & Stokes, M. D. (2002). Scale dependence of bubble creation mechanisms in breaking waves. *Nature*, *418*.

Derakhti, M., Thomson, J., Bassett, C. S., Malila, M. P., & Kirby, J. T. (2024, feb). Statistics of bubble plumes generated by breaking surface waves. *J. Geophys. Res.*, *accepted*. Retrieved from https://doi.org/10.22541/essoar.167751591.11265648/v1 doi: 10.22541/essoar.167751591.11265648/v1

Dobson, F., Perrie, W., & Toulany, B. (1989). On the deep-water fetch laws for wind-generated surface gravity waves. *Atmos.-Ocean*, *27*, 210-236.

Dragan-Górska, A., Gorska, N., Markuszewski, P., & Klusek, Z. (2023). Influence of wind and waves on ambient noise and bubble entrainment depth in the semi-enclosed baltic sea. *Oceanologia*. Retrieved from https://www.sciencedirect.com/science/article/pii/S0078323423000921 doi: https://doi.org/10.1016/j.oceano.2023.12.003

Ellenson, A., & Özkan-Haller, H. T. (2018). Predicting large ocean wave events characterized by bimodal energy spectra in the presence of a low-level southerly wind feature. *Weather and Forecasting*, *33*(2), 479-499. Retrieved from https://doi.org/10.1175/WAF-D-17-0035.1 doi: 10.1175/WAF-D-17-0035.1

Farmer, D. M., & Vagle, S. (1989). Waveguide propagation of ambient sound in the ocean-surface bubble layer. *The Journal of the Acoustical Society of America*, *86*(5), 1897-1908. Retrieved from https://doi.org/10.1121/1.398568 doi: 10.1121/1.398568

Felizardo, F., & Melville, W. (1995). Correlation between ambient noise and the ocean surface wave field. *J. Phys. Oceanogr.*, *25*, 513-532.

Fontaine, E. (2012, 2013/04/06). A theoretical explanation of the fetch- and duration-limited laws. *J. Phys. Oceanogr.*, *43*(2), 233–247. doi: 10.1175/JPO-D-11-0190.1

Freeland, H. (2007). A short history of Ocean Station Papa and Line P. *Progress in Oceanography*, *75*, 120-125.

Gemmrich, J. (2010). Strong turbulence in the wave crest region. *J. Phys. Oceanogr.*, *40*, 583-595. Retrieved from DOI:10.1175/2009JPO4179.1

Hasselmann, K., Barnett, T. P., Bouws, E., Carlson, H., Cartwright, D. E., Enke, K., ... others (1973). Measurements of wind-wave growth and swell decay during the joint north sea wave project (jonswap). *Ergaenzungsheft zur Deutschen Hydrographischen Zeitschrift, Reihe A*.

Hildebrand, J. A., Frasier, K. E., Baumann-Pickering, S., & Wiggins, S. M. (2021, 06). An empirical model for wind-generated ocean noise. *The Journal of the Acoustical Society of America*, *149*(6), 4516-4533. Retrieved from https://doi.org/10.1121/10.0005430 doi: 10.1121/10.0005430

Lemon, D. D., Farmer, D. M., & Watts, D. R. (1984). Acoustic measurements of wind speed and precipitation over a continental shelf. *J. Geophys. Res.*, *89*(C3), 3462-3472.

Manasseh, R., Babanin, A. V., Forbes, C., Rickards, K., Bobevski, I., & Ooi, A. (2006, 04). Passive Acoustic Determination of Wave-Breaking Events and Their Severity across the Spectrum. *Journal of Atmospheric and Oceanic Technology*, *23*(4), 599-618. Retrieved from https://doi.org/10.1175/JTECH1853.1 doi: 10.1175/JTECH1853.1

Na, B., Chang, K.-A., Huang, Z.-C., & Lim, H.-J. (2016). Turbulent flow field and air entrainment in laboratory plunging breaking waves. *Journal of Geophysical Research: Oceans*, n/a–n/a. Retrieved from http://dx.doi.org/10.1002/2015JC011377 doi: 10.1002/2015JC011377

Pierson, W. J., & Moskowitz, L. (1964). A proposed spectral form for fully developed wind seas based on the similarity theory of A. A. Kitaigorodskii. *J. Geophys. Res.*, *69*, 5181–5190.

Portilla-Yandún, J. (n.d.). The global signature of ocean wave spectra. *Geophysical Research Letters*, n/a–n/a. Retrieved from http://dx.doi.org/10.1002/2017GL076431 (2017GL076431) doi: 10.1002/2017GL076431

Schwendeman, M., & Thomson, J. (2014, 2015/01/21). A horizon-tracking method for shipboard video stabilization and rectification. *Journal of Atmospheric and Oceanic Technology*, *32*(1), 164–176. Retrieved from http://dx.doi.org/10.1175/JTECH-D-14-00047.1 doi: 10.1175/JTECH-D-14-00047.1

Schwendeman, M., Thomson, J., & Gemmrich, J. (2014). Wave breaking dissipation in a young wind sea. *J. Phys. Oceanogr.*, *44*(1), 104-127.

Stiassnie, M. (2012, 02). Fetch-limited growth of wind waves. *J. Geophys. Res.*, *117*. doi: 10.1029/2011JC007579

Strand, K. O., Breivik, Ø., Pedersen, G., Vikebø, F. B., Sundby, S., & Christensen, K. H. (2020). Long-term statistics of observed bubble depth versus modeled wave dissipation. *Journal of Geophysical Research: Oceans*, *125*(2), e2019JC015906. Retrieved from https://agupubs.onlinelibrary.wiley.com/doi/abs/10.1029/2019JC015906 (e2019JC015906 10.1029/2019JC015906) doi: https://doi.org/10.1029/2019JC015906

Sutherland, P., & Melville, W. K. (2013). Field measurements and scaling of ocean surface wave-breaking statistics. *Geophysical Research Letters*, n/a–n/a. Retrieved from http://dx.doi.org/10.1002/grl.50584 doi: 10.1002/grl.50584

Sutherland, P., & Melville, W. K. (2015, 2015/04/28). Field measurements of surface and near-surface turbulence in the presence of breaking waves. *Journal of Physical Oceanography*, *45*(4), 943–965. Retrieved from http://dx.doi.org/10.1175/JPO-D-14-0133.1 doi: 10.1175/JPO-D-14-0133.1

Thomson, J. (2012). Wave breaking dissipation observed with SWIFT drifters. *Journal of Atmospheric and Oceanic Technology*, *29*(12), 1866–1882. Retrieved from https://doi.org/10.1175/JTECH-D-12-00018.1 doi: 10.1175/JTECH

-D-12-00018.1

Thomson, J., D'Asaro, E. A., Cronin, M., Rogers, E., Harcourt, R., & Schcerbina, A. (2013). Waves and the equilibrium range at Ocean Weather Station P. *J. Geophys. Res.*, *118*, 1-12. Retrieved from https://agupubs.onlinelibrary.wiley.com/doi/full/10.1002/2013JC008837 doi: https://doi.org/10.1002/2013JC008837

Thomson, J., & Jessup, A. (2009). A fourier-based method for the distribution of breaking crests from video observations. *J. Atmos. Ocean. Tech.*, *26*.

Thomson, J., & Rogers, W. E. (2014). Swell and sea in the emerging Arctic Ocean. *Geophysical Research Letters*, n/a–n/a. Retrieved from http://dx.doi.org/10.1002/2014GL059983 doi: 10.1002/2014GL059983

Thomson, J., Schwendeman, M. S., Zippel, S. F., Moghimi, S., Gemmrich, J., & Rogers, W. E. (2016). Wave-breaking turbulence in the ocean surface layer. *Journal of Physical Oceanography*, *46*(6), 1857-1870. Retrieved from http://dx.doi.org/10.1175/JPO-D-15-0130.1 doi: 10.1175/JPO-D-15-0130.1

Thomson, J., Talbert, J., de Klerk, A., Brown, A., Schwendeman, M., Goldsmith, J., ... Meinig, C. (2015, 2015/06/18). Biofouling effects on the response of a wave measurement buoy in deep water. *Journal of Atmospheric and Oceanic Technology*, *32*(6), 1281–1286. Retrieved from http://dx.doi.org/10.1175/JTECH-D-15-0029.1 doi: 10.1175/JTECH-D-15-0029.1

Urick, R. J. (1975). *Principles of Underwater Sound*. McGraw-Hill, New York.

Voermans, J. J., Smit, P. B., Janssen, T. T., & Babanin, A. V. (2020). Estimating wind speed and direction using wave spectra. *Journal of Geophysical Research: Oceans*, *125*(2), e2019JC015717. Retrieved from https://agupubs.onlinelibrary.wiley.com/doi/abs/10.1029/2019JC015717 (e2019JC015717 10.1029/2019JC015717) doi: 10.1029/2019JC015717

Wenz, G. (1962). Acoustic ambient noise in the ocean: Spectra and sources. *J. Acoust. Soc. Am.*, *34*, 1936-1956.

Yang, J., Nystuen, J. A., Riser, S. C., & Thorsos, E. I. (2023). Open ocean ambient noise data in the frequency band of 100 hz to 50 khz from the pacific ocean. *JASA Express Letters*, *3*(3), 036001. Retrieved from https://doi.org/10.1121/10.0017349 doi: 10.1121/10.0017349